

# Forecasting Constraints on Cosmology and Modified Gravitational-wave Propagation by Strongly Lensed Gravitational Waves Associating with Galaxy Surveys

Anson Chen<sup>1, a</sup> and Jun Zhang<sup>1, 2</sup>

<sup>1</sup>*International Center for Theoretical Physics Asia-Pacific,  
University of Chinese Academy of Sciences, 100190 Beijing, China*

<sup>2</sup>*Taiji Laboratory for Gravitational Wave Universe,  
University of Chinese Academy of Sciences, 100049 Beijing, China*

(Dated: February 13, 2026)

Gravitational lensing of gravitational wave (GW) will become the next frontier in studying cosmology and gravity. While time-delay cosmography using quadruply lensed GW events associated with optical images of the lens systems can provide precise measurement of the Hubble constant ( $H_0$ ), they are considered to be much rarer than doubly lensed events. In this work, we analyze time-delay cosmography with doubly lensed GW events for the first time. We generate mock doubly lensed GW events with designed sensitivity of the LIGO-Virgo-KAGRA (LVK) O5 network, with LIGO post-O5 upgrade, and with Einstein Telescope (ET) + Cosmic Explorer (CE) respectively, and select the events that can be associated with future galaxy surveys. Over 1000 realizations, we find an average of 0.2(2.4) qualified events with the LVK O5(post-O5) network. Whereas with the ET+CE network, we find an average of 73.2 qualified events over 100 realizations. Using the Singular Isothermal Sphere (SIS) lens model, we forecast the constraints on cosmological parameters and modified GW propagation by combining time-delay cosmography and the standard siren approach. The average posterior gives a constraint on  $H_0$  with a relative uncertainty of 14%, 10% and 0.42% in the  $\Lambda$ CDM model for the LVK O5, LVK post-O5, and ET+CE network, respectively. While the LVK network gives uninformative constraints on the  $(w_0, w_a)$  dynamical dark energy model, the ET+CE network yields a moderate constraint of  $w_0 = -1.02^{+0.31}_{-0.22}$  and  $w_a = 0.48^{+0.99}_{-1.54}$ . In addition, our method can provide precise constraints on modified GW propagation effects jointly with  $H_0$ .

## I. INTRODUCTION

Despite of the great success of the Lambda Cold Dark Matter ( $\Lambda$ CDM) standard cosmology model, it is facing many challenges today. For instance, the second data release of the Dark Energy Spectroscopic Instrument (DESI) indicates that a dynamical dark energy model is favored by the Baryon acoustic oscillation (BAO) data, combined with data from the cosmic microwave background (CMB) and supernovae observations [1, 2]. It challenges the assumption of the  $\Lambda$ CDM model, where dark energy is interpreted as the Cosmological Constant. In addition, the Hubble tension problem has long existed between the CMB data and the local universe measurements, e.g.  $H_0 = 67.49 \pm 0.50 \text{ km s}^{-1}\text{Mpc}^{-1}$  from the Planck mission [3] and  $H_0 = 74.03 \pm 1.42 \text{ km s}^{-1}\text{Mpc}^{-1}$  from the SH0ES collaboration [4], which may hint for new physics beyond the  $\Lambda$ CDM model (see review in [5]). To further examine whether such observational anomalies are caused by systematics or unknown fundamental physics, more data from various aspects of observations are required in the near future.

On the other hand, gravitational wave (GW) detection has provided a unique laboratory in cosmological research. The latest Gravitational-Wave Transient Catalog 4.0 (GWTC-4) released by the LIGO-Virgo-KAGRA collaboration (LVK) reported 128 new compact binary coalescence (CBC) events from the first part of the fourth

LVK observing run (O4a) [6], which adds up the total number of CBC events to 218. These events can provide an independent measurement of  $H_0$ , as well as cosmological propagation effects, with the standard siren method [7–13]. For instance, the combination of the GW170817 bright siren event and the dark siren analysis for 142 of the GWTC-4 events yields  $H_0 = 76.6^{+13.0}_{-9.5} \text{ km s}^{-1}\text{Mpc}^{-1}$  [12]. As more CBC events will be detected by the next-generation (XG) detectors in the future, such as Einstein Telescope (ET) [14] and Cosmic Explorer (CE) [15], the error of  $H_0$  measurement by the dark siren method can be reduced to lower than 1% [16, 17]. With such precision in  $H_0$  measurements, GWs are expected to provide a new perspective in solving the Hubble tension problem in the near future.

Apart from the standard siren method,  $H_0$  can also be measured with GW detections in other aspects, in particular the gravitational lensing of GWs [18–21]. The time-delay cosmography with strong lensing has been applied in electromagnetic (EM) observations in the past few decades [22–27]. For example, the TD-COSMO Collaboration obtained the latest constraints  $H_0 = 71.6^{+3.9}_{-3.3} \text{ km s}^{-1}\text{Mpc}^{-1}$  with 8 strongly lensed quasars [28]. On the other hand, GW signals can also be lensed by foreground galaxies, and result in multiple images for the same event. It has been proposed that these strongly lensed GW events can provide accurate measurements of  $H_0$ , in association with strongly lensed images of their host galaxies. However, it requires precise estimation of the Fermat potential, which can either be obtained by strongly lensed EM counterparts of the

<sup>a</sup> chena@ucas.ac.cn

events [29], or by more than two images of the lensed events [19, 21]. These special events are considered to be rare in future detections, where 70% of the strongly lensed events are expected to have only two images [30]. Therefore, the chances to obtain cosmological constraints with these special strongly lensed events by LVK detections are very small.

In this work, we propose an alternative method to measure cosmological parameters with doubly lensed GW events, associating with images of the strong lensing systems observed by large-scale galaxy surveys. The latest survey performed by the Euclid satellite is expected to discover about 75,000 strong lensing systems [31], and the Legacy Survey of Space and Time (LSST) to be carried out by the Vera C. Rubin Observatory is also expected to detect about 70,000 strong lensing systems [32]. The database of these strongly lensed galaxies can provide a precise map to identify the host galaxies of strongly lensed GW events. Using the Singular Isothermal Sphere (SIS) lens model, one can infer the Einstein radius  $\theta_E$  from the angles between the two images of the source galaxy and the lens galaxy in a strong-lensing system. In addition to  $\theta_E$ , with the redshifts of the lens and the source galaxy, we can estimate  $H_0$  using time-delay cosmography with strongly lensed GW signals, as well as dark energy or cosmological modified gravity effects described by the  $(\Xi_0, n)$  parameterization or the Horndeski-class parameterization [33–40]. Apart from this, the luminosity distance of the GW event and the redshift of the source galaxy can provide a standard siren measurement of the cosmological parameters jointly with time-delay cosmography. The main uncertainty of the time-delay cosmography comes from the impact parameter  $y$ , which can be jointly estimated from the two lensed GW signals.

The structure of this paper is listed as followed. Section II introduces the theoretical framework of strong lensing with the SIS model, cosmology models, and modified GW propagation. Section III describes our method to infer constraints on cosmological parameters. Section IV presents the mock data simulation we perform to obtain the cosmological constraints, and the inference results are shown in Section V. Finally, we summarize our work in Section VI.

## II. THEORETICAL FRAMEWORK

### A. Strong-lensing with the SIS model

It has been shown in literature that the eccentricity and detailed radial-mass distribution of the lens galaxy make a relatively small impact to lens statistic and cosmological implication [18, 41–43] (although  $H_0$  measurement would be sensitive to lens models given a fixed lens mass and Einstein radius). We therefore use the SIS lens model to perform cosmography in this work. The SIS model describes the galaxy mass distribution by assuming that the behavior of stars and other mass components

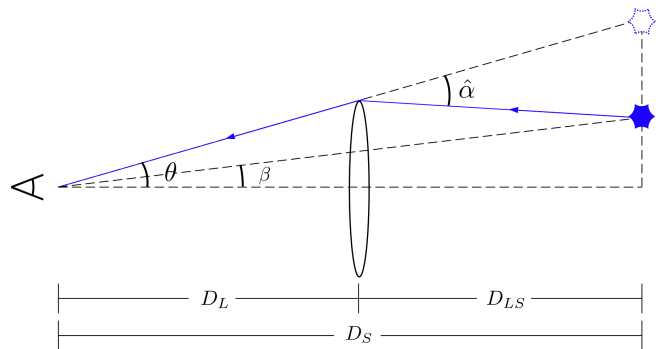


FIG. 1: Schematic figure for strong-lensing with the thin-lens approximation.

of the galaxy are similar to ideal gas particles in an adiabatic system [44]. The density profile of the SIS model is given by

$$\rho(r) = \frac{\sigma_v^2}{2\pi G} \frac{1}{r^2}, \quad (2.1)$$

where  $\sigma_v$  is the velocity dispersion. The Einstein radius of the SIS model is given by [45]

$$\theta_E = 4\pi \frac{\sigma_v^2}{c^2} \frac{D_{LS}}{D_S}, \quad (2.2)$$

where  $D_{LS}$  and  $D_S$  are the angular diameter distances between the lens and the source, and between the observer and the source respectively. The lens mass for the SIS model is further given by [45]

$$M_L = 4\pi \frac{\sigma_v^4}{Gc^2} \frac{D_L D_{LS}}{D_S}, \quad (2.3)$$

where  $D_L$  is the angular diameter distance from the observer to the lens. Therefore one can obtain the relation

$$\theta_E^2 = 4\pi \frac{GM_L}{c^2} \frac{D_{LS}}{D_L D_S}. \quad (2.4)$$

In addition, a special feature of the SIS model is that the reduced deflection angle<sup>1</sup>  $\alpha$  equals to  $\theta_E$ , so that the lens equation becomes

$$\theta_{\pm} = \beta \pm \theta_E, \quad (2.5)$$

where  $\theta_{\pm}$  stands for the angles between the two images and the lens on the line-of-sight, and  $\beta$  is the true source angular position (see Figure 1). If  $\beta < \theta_E$ , there exists two images. Otherwise, there is only one image. Therefore, one can directly obtain the Einstein radius  $\theta_E = (\theta_+ - \theta_-)/2$  for the doubly lensed system, which is half of the angle between the two images in observations.

<sup>1</sup> The reduced deflection angle  $\alpha$  relates to the deflection angle  $\hat{\alpha}$  in Figure 1 by  $\alpha = \hat{\alpha} D_{LS}/D_S$ .

On the other hand, the time delay of the lensed signals is given by

$$t_d(\vec{\theta}, \vec{\beta}) = \frac{1+z_L}{c} \frac{D_L D_S}{D_{LS}} \left[ \frac{1}{2} (\vec{\theta} - \vec{\beta})^2 - \psi(\vec{\theta}) \right], \quad (2.6)$$

where  $\psi(\vec{\theta})$  is the effective potential of the lens, and it causes the Shapiro time delay of the signals. The time delay can also be written in terms of dimensionless quantities:

$$t_d(\vec{x}, \vec{y}) = \frac{1+z_L}{c} \frac{D_L D_S}{D_{LS}} \theta_E^2 T(\vec{x}, \vec{y}), \quad (2.7)$$

where  $\vec{x} = \vec{\theta}/\theta_E$  and  $\vec{y} = \vec{\beta}/\theta_E$  are dimensionless relative position of the image and the source. In the SIS system, the dimensionless time delay for the two images is given by [46]

$$T_{\pm} = \mp y - \frac{1}{2}. \quad (2.8)$$

The uncertainty of time delay measurement in EM strong lensing is a significant contribution to the uncertainty in cosmological constraint [24]. Meanwhile, the arrival time of GW signals can be precisely measured, so the observed time delay measurement uncertainty in GW lensing is greatly reduced.

For gravitationally lensed GWs, the waveform is modified by  $\tilde{h}_L(f) = F(\omega)\tilde{h}(f)$  in the frequency domain, where  $F(\omega)$  is called the amplification factor ( $\omega = 2\pi f$ ). In the region of CBC GWs lensed by galaxies, the wavelength of GWs is much lower than the lens size and satisfies  $|\Delta t_d \cdot \omega| \gg 1$ , so we can use the geometric optic approximation of  $F(\omega)$ , given by [45, 47]

$$F(\omega) \simeq \sum_j \sqrt{|\mu_j|} \exp\left(i\omega t_{d,j} - i \text{sign}(\omega) n_j \frac{\pi}{2}\right), \quad (2.9)$$

where  $\mu_j$  is the magnification factor for the  $j$ -th image, and  $n_j = 0, 1, 2$  for the type I, II, III image respectively. In the SIS model, the magnification factor is given by [46]

$$\mu_{\pm} = 1 \pm \frac{1}{y}. \quad (2.10)$$

For lensed GWs, the waveform amplitude is multiplied by  $|\mu_{\pm}|$ , which introduces bias in the observed GW luminosity distance  $d_L^{\text{GW}}$ . Therefore, one can first obtain  $y$  by the ratio of the lensed signal,

$$y = \frac{\mu_+/\mu_- + 1}{\mu_+/\mu_- - 1}. \quad (2.11)$$

so that the lensing magnification can be removed from the lensed signals with equation (2.10), and the true  $d_L^{\text{GW}}$  can be obtained. In our analysis, we will jointly estimate  $d_L^{\text{GW}}$  and  $y$  with the two images of lensed GW signals (as shown in Section IV C).

For higher  $y$  within  $y < 1$ , the amplitude of the second image of lensed GWs is suppressed, so its signal-to-noise ratio (SNR) could be below the detection threshold, typically  $\rho_{\text{th}} = 8$ . Fortunately, with sub-threshold signal searching techniques, lensed signals can be digged out with SNR down to 4 [48–52], which greatly improve the chance to find strongly-lensed signal pairs.

## B. Cosmology model and Modified Gravitational-wave propagation

With strongly-lensed GWs, we can estimate cosmological parameters and modified gravity parameters that affect GW propagation. In a flat universe described by the Friedman-Lemaître-Robertson-Walker (FLRW) Metric, the luminosity distance of an EM source at redshift  $z$  is given by [53]

$$d_L = (1+z) \int_0^z \frac{c dz'}{H_0 E(z')}. \quad (2.12)$$

For the  $\Lambda$ CDM model,  $E(z) = \sqrt{\Omega_{m,0}(1+z)^3 + \Omega_{\Lambda,0}}$ , where  $\Omega_{m,0}$  and  $\Omega_{\Lambda,0}$  are the energy density of matter and dark energy today (the radiation energy density is negligible in the late-time universe). The angular diameter distance is related to the luminosity distance by  $d_A = d_L/(1+z)^2$ .

However, dark energy can be dynamical over time, instead of a constant in the  $\Lambda$ CDM model. A simple parameterization of the equation of state of dynamical dark energy is the Chevallier-Polarski-Linder (CPL) parametrization [54, 55], which depends on the scale factor  $a$  by

$$w(a) = w_0 + w_a(1+a). \quad (2.13)$$

The corresponding  $E(z)$  is given by

$$E(z) = \sqrt{\Omega_{m,0}(1+z)^3 + \Omega_{\Lambda,0}(1+z)^{3(1+w_0+w_a)} e^{-\frac{3w_a z}{(1+z)}}}. \quad (2.14)$$

The  $\Lambda$ CDM model is recovered by  $w_0 = -1$  and  $w_a = 0$ . The first two BAO data releases by DESI show a preference for the CPL dark energy model over the  $\Lambda$ CDM model by over  $2.8\sigma$  for the first time, combining with CMB data and supernovae data [1, 2].

The nature of dark energy remains a mystery nowadays, yet many explanations to it have been proposed. Modified gravity is one of the popular dark energy theories. In a general modified gravity framework, the propagation of GW would deviate from General Relativity (GR), making GW a unique probe to dark energy. Meanwhile, the GW propagation speed has been tightly constrained by the multi-messenger event GW170817 to be consistent to GR<sup>2</sup> [59–61]. Therefore, the remain-

<sup>2</sup> Some theories predict a transition in GW speed at a lower energy scale than the LVK detection band, but it can be constrained by LISA in the future [56–58].

ing propagation effect without strong constraints is the damping effect<sup>3</sup>, as described in the GW propagation equation [33, 34, 63–65]:

$$\tilde{h}_A'' + 2\mathcal{H}[1 - \delta(\eta)]\tilde{h}_A' + c^2 k^2 \tilde{h}_A = 0, \quad (2.15)$$

where  $\tilde{h}_A(\eta, k)$  is GW in Fourier space, the subscript  $A$  denotes the  $+$  or  $\times$  GW polarization,  $\eta$  is the conformal time,  $'$  denotes the derivative with respect to  $\eta$ , and  $\mathcal{H} = a'/a$  is the conformal Hubble parameter. The term  $\delta(\eta)$  is the extra damping effect induced by modified gravity, and GR is recovered at  $\delta(\eta) = 0$ . By solving equation (2.15), one can find the ratio between the modified GW luminosity distance and the EM luminosity distance as defined in equation (2.12),

$$\frac{d_L^{\text{GW}}(z)}{d_L^{\text{EM}}(z)} = \exp \left[ - \int_0^z \frac{dz'}{1+z'} \delta(z') \right]. \quad (2.16)$$

The explicit form of  $\delta(z)$  can be derived in specific modified gravity frameworks<sup>4</sup>. But one widely-used general parameterization originated from non-local modified gravity models is given by [68, 69]

$$\frac{d_L^{\text{GW}}(z)}{d_L^{\text{EM}}(z)} = \Xi_0 + \frac{1 - \Xi_0}{(1+z)^n}, \quad (2.17)$$

where  $\Xi_0$  and  $n$  are constants. At  $z = 0$ , the distance ratio is 1, and it approaches the constant  $\Xi_0$  as  $z$  increases, which describes the deviation from GR consistent with dark-energy driven expansion of the universe at low redshift. This parameterization can be mapped into different modified gravity models (see [34] for some examples). A first constraint on  $\Xi_0$  has been given by the dark siren method with GWTC-3 and GWTC-4 data [12, 37–39], though the uncertainty is large at this stage.

Another widely tested model is the alpha-basis parameterization built upon the Horndeski scalar-tensor theory framework, where deviation from GR at the linear perturbation level can be described by 4 parameters:  $\alpha_M, \alpha_K, \alpha_B$  and  $\alpha_T$  [70, 71]. While  $\alpha_T$  is the deviation of GW speed from  $c$ ,  $\alpha_M$  describes the running rate of the effective Planck mass, which leads to the extra damping factor by  $\delta(z) = -\alpha_M(z)/2$  [34]. The evolution of  $\alpha_M$  is often parameterized to be proportional to the growth of dark energy density,  $\alpha_M(z) = c_M \Omega_\Lambda(z)/\Omega_{\Lambda,0}$ . Taking the dark energy density evolution in the  $\Lambda$ CDM model, the distance ratio is given by

$$\frac{d_L^{\text{GW}}(z)}{d_L^{\text{EM}}(z)} = \exp \left\{ \frac{c_M}{2\Omega_{\Lambda,0}} \ln \frac{1+z}{[\Omega_{m,0}(1+z)^3 + \Omega_{\Lambda,0}]^{1/3}} \right\}. \quad (2.18)$$

<sup>3</sup> Though see [62] for correlation between GW speed and damping effect.

<sup>4</sup> See [66, 67] for a more general GW damping term that includes frequency-dependent modification.

The constant  $c_M$  has been constrained by the CMB and large-scale structures [72–74], as well as the dark siren method [12, 38, 39, 75]. Constraint of  $\Xi_0$  and  $c_M$  parameterization has also been proposed using quadruply lensed GW events [76, 77]. Meanwhile, it has been shown that the geometric optic time delay for modified GW propagation in scalar-tensor theories remains the same as in GR [78, 79].

### III. METHOD

In this work, we aim to obtain cosmological constraints with the doubly-lensed GW events and the lensed images of their host galaxies from strong lensing catalogues. Using the enhanced localization technique with the effective detector network consisting of ground-based GW detectors at different spacetime due to time delay of strongly lensed signals, the sky localization area of strongly lensed GWs can be tightly constrained to  $\Delta\Omega \sim 0.01 \text{ deg}^2$  [21], which greatly enhance our chances to find the corresponding strongly lensed host galaxies from galaxy surveys. In the case where there are more than one strongly lensed galaxies within the localization area, one can compare the Bayes factor between each system with the likelihood and identify the true lensed systems, which have been studied in previous works [19, 80]. Here we consider the optimistic case where true strongly lensed systems are identified for GW lensed events if their images can be resolved by galaxy surveys (See Section IV B for lensed event selection).

Given the redshift of the source galaxy and the GW luminosity distance  $d_L^{\text{GW}}$ , we can constrain cosmological parameters via the standard siren method. However, the first analysis of lensed GWs will result in biases in  $d_L^{\text{GW}}$  because of magnification. Therefore we need to re-analyze lensed GWs once the lensed signal pairs are confirmed. By joint re-analysis of the two images of lensed GWs, we can obtain the posterior samples of the true  $d_L^{\text{GW}}$  and the impact parameter  $y$  of lensed events. See Section IV C for details of waveform parameter re-analysis.

In addition, we can obtain cosmological constraints via time delay cosmography of strongly lensed GWs. Given the observed time delay between GW signal images,  $\Delta t = t_{d,2} - t_{d,1}$ , as well as redshifts of the lens galaxy and the source galaxy, the Einstein radius  $\theta_E$ , and the impact parameter  $y$ , we can estimate cosmological parameters with equation (2.7) and (2.8) using the SIS model. For the resolved image of a strong-lensing system in galaxy surveys, the angular separation between the two images of the source can be observed. Then one can obtain  $\theta_E$  of the SIS lensing system by  $\theta_E = (\theta_+ - \theta_-)/2 = \Delta\theta/2$ , given the lens equation (2.5). Therefore, we construct the log-likelihood on cosmological parameters  $\lambda$  with  $\chi^2$ -

statistics over  $N$  lensed events, given by

$$\log \mathcal{L}(\lambda) = -\frac{1}{2} \sum_{i=1}^N \chi^2(\lambda, \Delta t, \Delta \theta, z_L, z_S, y), \quad (3.1)$$

where

$$\chi^2(\lambda, \Delta t, \Delta \theta, z_L, z_S, y) = \left[ \frac{d_L^{\text{GW,obs}} - d_L^{\text{GW}}(\lambda, z_S)}{\delta d_L^{\text{GW,obs}}} \right]^2 + \left[ \frac{\Delta t^{\text{obs}} - \Delta t(\lambda, \Delta \theta, z_L, z_S, y)}{\delta(\Delta t)} \right]^2. \quad (3.2)$$

The uncertainty in time delay reconstruction is dominated by  $\delta y$  from GW re-analysis, which typically gives relative error of 10% – 20%. The uncertainty in other factors, namely  $\Delta \theta, z_L, z_S$ , is in order of a few percents from galaxy surveys<sup>5</sup>. Moreover, uncertainty in GW arrival time in milliseconds is negligible compared to time delay in days. Therefore we have  $\delta(\Delta t)/\Delta t \simeq \delta y/y$  in the likelihood. Using flat priors on  $\lambda$ , the posterior for  $\lambda$  can then be obtained by Bayesian inference with Markov Chain Monte Carlo (MCMC) sampling.

The aim of this work is to forecast cosmological constraints given observed lensed GW pairs. In practice, however, one must also consider the detectability of lensed GW pairs, and weight the likelihood of observables by selection effects. This should be analyzed explicitly in future works.

#### IV. SIMULATION

To forecast the cosmological constraints with doubly lensed GW events, we first simulate mock data for strongly lensed GW events based on theoretical models for GW source population, merger rate, and lensing rate. Next, we filter out the events that can be associated with strong-lensing systems based on the resolution, the sky coverage and the depth of galaxy surveys. We then perform joint parameter estimation for lensed GW signal pairs. Finally, we perform MCMC sampling to obtain constraints on cosmological parameters. Details of simulation in each step are clarified in the following sections.

##### A. Mock GW events

Our first step of simulation is generating mock GW data for the LVK O5 stage, the post-O5 stage, and the

<sup>5</sup> The redshift uncertainty from spectroscopic survey and photometric survey is expected to be in order of 0.1% and 1% respectively (e.g. [81]; [82]). Although photometric redshift of the source galaxy is affected by light bending due to gravitational lensing, follow-up spectroscopic survey could provide more accurate redshift measurement.

next-generation detectors ET+CE, using the Python tool `GWSim` [83]. We assume that the O5 detector network consists of LIGO Observatory at Livingston (L1) and Hanford (H1), Virgo (V1) and KAGRA (K1), with their designed sensitivity curves<sup>6</sup> [84] that we implement in `GWSim`. For the post-O5 detector network, we assume that LIGO India (A1) will join detections with LIGO designed sensitivity, so that there are 5 detectors in total. We also assume that post-O5 upgrades will be installed in L1 and H1 with the A# sensitivity<sup>7</sup>. For the ET+CE network, we use the orientation and the location of ET with the triangular configuration implemented in `Bilby`<sup>8</sup>, with a sensitivity curve for the 10 km arm length design<sup>9</sup>. We then assume two CE locating at L1 and H1 sites, with a sensitivity curve for the 40 km arm length design<sup>10</sup>. For each detector, we assume a duty cycle of 75%.

We generate the mock binary black hole (BBH) merger events using the “Powerlaw + Double Peak” black hole mass distribution model and the Madau-Dickinson redshift evolution model, which are used in GWTC-4 cosmology paper [12]. We only consider BBH here, since they compose of most of the GW events in LVK detections, while the event rates of binary neutron star and neutron-star-black-hole merger have large uncertainty. The description of these models and our injected values are shown in Appendix A. The luminosities of GW events are then generated from redshift with the fiducial  $\Lambda$ CDM model with  $H_0 = 67.8 \text{ km s}^{-1} \text{ Mpc}^{-1}$  and  $\Omega_{m,0} = 0.308$  from Planck 2018 TT, TE, EE+lowE+lensing+BAO results [3]. We assume 5 years of observations for each detector network configuration, and that GW events distribute uniformly in the sky map. We select mock events with  $\text{SNR} > 11$ , and proceed to lensed event generation.

##### B. Lensed event selection

We follow [18] to compute the optical depth for GW sources, which gives the probability for GW events being lensed at different redshifts (see detailed derivation in

<sup>6</sup> L1 and H1: <https://dcc.ligo.org/DocDB/0149/T1800042/005/AplusDesign.txt>  
V1: [https://git.ligo.org/publications/detectors/obs-scenarios-2019/blob/master/Scripts/Figure1/data/avirgo\\_O5high\\_NEW.txt](https://git.ligo.org/publications/detectors/obs-scenarios-2019/blob/master/Scripts/Figure1/data/avirgo_O5high_NEW.txt)  
K1: [https://git.ligo.org/publications/detectors/obs-scenarios-2019/blob/master/CurvesForSimulation/kagra\\_128Mpc.txt](https://git.ligo.org/publications/detectors/obs-scenarios-2019/blob/master/CurvesForSimulation/kagra_128Mpc.txt)  
<sup>7</sup> [https://dcc.ligo.org/LIGO-T2300041-v1/public/Asharp\\_strain.txt](https://dcc.ligo.org/LIGO-T2300041-v1/public/Asharp_strain.txt)  
<sup>8</sup> <https://git.ligo.org/lscsoft/bilby/-/blob/d37609ccc9a878750c841b4b93da990e63acffb2/bilby/gw/detector/detectors/ET.interferometer>  
<sup>9</sup> <https://apps.et-gw.eu/tds/ql/?c=16492/ET10kmcolumns.txt>  
<sup>10</sup> [https://dcc.cosmicexplorer.org/CE-T2000017/public/cosmic\\_explorer\\_strain.txt](https://dcc.cosmicexplorer.org/CE-T2000017/public/cosmic_explorer_strain.txt)

Appendix B). The optical depth  $\tau$  is given by

$$\tau = \frac{F_*}{30} [D_S(1+z_S)]^3 y_{\max}^2 \left\{ 1 - \frac{1}{7} \frac{\Gamma[(8+\alpha)/\beta]}{\Gamma[(4+\alpha)/\beta]} \frac{\Delta t_*}{T_{\text{obs}}} \right\}, \quad (4.1)$$

where

$$F_* = 16\pi^3 n_{*,0} \left( \frac{\sigma_{*,0}}{c} \right)^4 \frac{\Gamma[(4+\alpha)/\beta]}{\Gamma[\alpha/\beta]}, \quad (4.2)$$

$$\Delta t_* = 32\pi^2 \left( \frac{\sigma_{*,0}}{c} \right)^4 \frac{D_S}{c} (1+z_S) y_{\max}. \quad (4.3)$$

$D_S$  and  $z_S$  are the angular diameter distance and redshift of the source,  $\Gamma$  is the Euler gamma function, and  $T_{\text{obs}}$  is the observation time of GW detectors. We adopt the modified Schechter function parameters as  $n_{*,0} = 8.0 \times 10^{-3} h^3 \text{Mpc}^{-3}$ ,  $\sigma_{*,0} = 144 \text{ km s}^{-1}$ ,  $\alpha = 2.49$ , and  $\beta = 2.29$ , following previous study in [18] (also consistent with recent studies, e.g. in [85–87]).

The maximal impact parameter  $y_{\max}$  depends on the SNR detection threshold  $\rho_{\text{th}}$  and the SNR of the unlensed GW signal  $\rho_{\text{UL}}$  by

$$y_{\max} = \left[ \left( \frac{\rho_{\text{th}}}{\rho_{\text{UL}}} \right)^2 + 1 \right]^{-1} \quad (4.4)$$

In our simulation, we generate GW events with  $\text{SNR} > 11$ , so we take  $\rho_{\text{UL}} = 11$  for simplicity. As discussed in Section II A, we can take  $\rho_{\text{th}} = 4$  for sub-threshold signal search. Therefore we have  $y_{\max} = 0.883^{11}$ . We randomly select lensed events from the mock GW catalogues weighted by the optical depth.

For the selected lensed events, we create the foreground galaxy lenses based on the stellar mass distribution of galaxies. We adopt the double-Schechter function to describe the galaxy density profile in stellar mass:

$$\Phi(M) = \exp\left(-\frac{M}{M^*}\right) \left[ \Phi_1^* \left(\frac{M}{M^*}\right)^{\alpha_1+1} + \Phi_2^* \left(\frac{M}{M^*}\right)^{\alpha_2+1} \right]. \quad (4.5)$$

We adopt  $\log(M^*/M_{\odot}) = 10.79$ ,  $\log(\Phi_1^*/h^3 \text{Mpc}^{-3}) = -3.31$ ,  $\log(\Phi_2^*/h^3 \text{Mpc}^{-3}) = -2.01$ ,  $\alpha_1 = -1.69$ , and  $\alpha_2 = -0.79$  from [88], and randomly draw lens galaxy stellar masses with probability weighted by equation (4.5). We then obtain the lens masses by assuming that stellar mass contributes to 10% of the galaxy total mass including dark matter halo. In addition, we draw lens redshifts  $z_L$  with probability weighted by the differential comoving volume  $dV_c/dz$ , and draw impact parameter  $y$  with probability weighted by  $y$  in  $(0, y_{\max})$ .

---

<sup>11</sup> Events with  $\rho_{\text{UL}} < 11$  in lensing systems with small  $y$  could also be detected, but  $y_{\max}$  for these systems are also small, so that their lensing probabilities are small. Our lensed event number can be considered as a conservative estimation.

Since our method relies on the resolved images of lensed host galaxies, we need to filter out the lensed events whose EM counterparts are observable and resolvable in galaxy surveys. We target the LSST survey, which will cover redshift up to 3 and a sky area of  $18000 \text{ deg}^2$  [82, 89], which is about 43% of the sky, so we only keep the same portion of events out of all mock events. In addition, the resolvable angle for the LSST camera is 0.2 arcsecond [90]. For the rest of lensed events, we compute  $\theta_E$  with equation (2.4) from  $M_L$  and  $D_L$ ,  $D_S$ ,  $D_{LS}$  converted from  $z_L$  and  $z_S$  with the fiducial  $\Lambda\text{CDM}$  model. Then we select resolvable lensed events with  $\theta_{\pm} = (y \pm 1)\theta_E > 0.2''$ .

We simulate 1000 realizations for LVK O5 and post-O5 observations. For the O5 run, we obtain at least one lensed events in 741 realizations. Considering events in the LSST's footprint, the average lensed event number is 0.55 over all 1000 realizations. However, we only obtain resolvable lensed events by LSST in 181 realizations after filtering, with an average of 0.20 resolvable events across all realizations. For the post-O5 run, we obtain resolvable lensed events in 912 realizations. Compared to an average of 7.8 total lensed events within LSST coverage, there are only 2.4 resolvable events across all realizations. For the ET+CE network, we obtain an average of 190.8 total lensed events, and 73.2 resolvable events in all of the 100 realizations. In our simulation, the fraction of resolvable lensed events by LSST is 31%-38%, which is consistent to the lensed event localization study by [80].

### C. Waveform parameter estimation

For each resolvable lensed event detected by LVK, we perform waveform parameter estimation (PE) jointly for the two signal images. We assume that both signals from a lensed event have been analyzed individually prior to our analysis, so that parameters like sky location, spin, time and phase at merger have been measured, which can be fixed in the re-analysis. So we only estimate parameters affected by strong lensing, which are chirp mass  $\mathcal{M}_c$ , mass ratio  $q$ , GW luminosity distance  $d_L^{\text{GW}}$ , and inclination angle  $\iota$  since it degenerates with  $d_L^{\text{GW}}$ . We also jointly estimate the impact parameter  $y$ . We first generate the unlensed waveform signal in frequency domain using the IMRPhenomXPHM waveform [91], and then create the two lensed signal images magnified by  $\mu_{\pm}(y)$  with equation (2.10) and a phase difference of  $\pi/2$  between images. For simplicity, we generate spin-free waveforms. The posterior of waveform parameters  $\{\phi\}$  given image data  $x_{j=1,2}$  in the joint analysis is thus given by

$$P(\phi|x_1, x_2) = \int P(x_1, x_2|\phi)\Pi(\phi)d\phi, \quad (4.6)$$

where  $\Pi(\phi)$  is the prior, and the joint log likelihood is given by

$$\log P(x_1, x_2|\phi) = -\frac{1}{2} \sum_{j=1}^2 \langle \tilde{h}(x_j) - \tilde{h}(\phi) | \tilde{h}(x_j) - \tilde{h}(\phi) \rangle. \quad (4.7)$$

Here  $f$  is the frequency,  $\tilde{h}(f)$  is the detector response to GW signals, given by

$$\tilde{h}(f) = \sum_k [F_+^k \tilde{h}_+(f) + F_\times^k \tilde{h}_\times(f)], \quad (4.8)$$

where  $F_+^k$  and  $F_\times^k$  are the antenna pattern functions of the  $k$  detector for the plus and cross GW polarization. The scalar product  $\langle \tilde{h}(f) | \tilde{g}(f) \rangle$  is defined as

$$\langle \tilde{h}(f) | \tilde{g}(f) \rangle \equiv 2 \operatorname{Re} \left[ \int df \frac{\tilde{h}(f) \tilde{g}^*(f) + \tilde{h}^*(f) \tilde{g}(f)}{\operatorname{Sn}(f)} \right], \quad (4.9)$$

where  $\operatorname{Sn}(f)$  is the power spectral density (PSD) of the detector noise. The priors on  $d_L^{\text{GW}}$  and  $y$  are  $\Pi(d_L^{\text{GW}}) \propto (d_L^{\text{GW}})^2$  and  $\Pi(y) \propto y$  respectively, while the priors for other parameters are uniform. Finally, the posterior samples are inferred with `nessai` [92, 93], which incorporates normalising flows in nested sampling within the `Bilby` package [94].

Figure 2 shows an example of the posterior samples from joint PE for lensed GW signals. We can see that, in spite of moderate degeneracy, the true  $d_L^{\text{GW}}$  and  $y$  are well recovered, and their marginalized posteriors generally follow Gaussian distribution. We can therefore obtain the observables and their uncertainties from the mean and the standard deviation of the posterior samples, respectively.

For the ET+CE network, however, the waveform parameter estimation is computationally expensive given a large event number. We thus perform Fisher matrix analysis to forecast the uncertainty of the waveform parameters for the ET+CE events, which is given by the square root of the diagonal elements of the covariance matrix  $\Sigma^{ij}$ . The Fisher matrix is the inverse of the covariance matrix, constructed by  $(\Sigma^{ij})^{-1} = \langle \partial \tilde{h} / \partial \phi_i | \partial \tilde{h} / \partial \phi_j \rangle$ . We numerically compute the partial derivatives of the waveform by finite differencing. The joint Fisher matrix for the two lensed GW signals is the sum of the Fisher matrices for the individual signals.

## V. RESULTS

We infer the posterior for cosmological parameters with equation (3.1) and (3.2) from all qualified lensed GW events in each realization using MCMC sampling with the `emcee` package [95]. For each realization, we estimate the posterior probability density function (PDF) from marginalized posterior samples with the Gaussian Kernel Density Estimation (KDE) method using

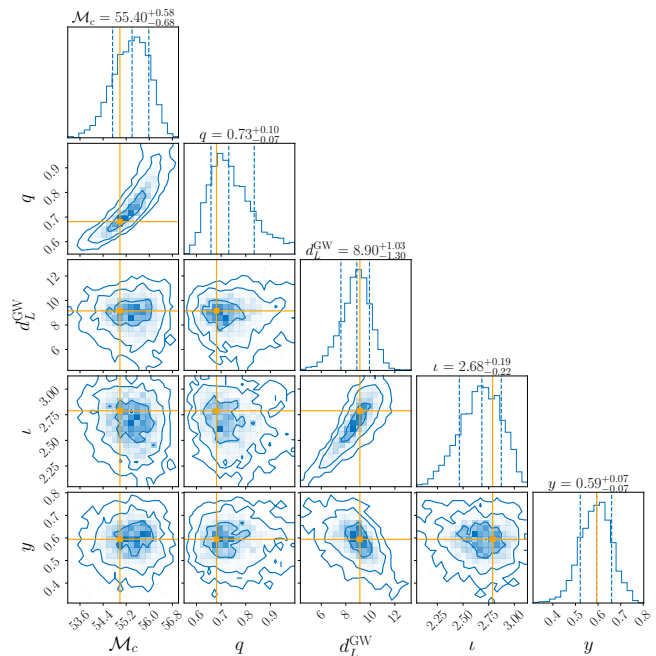


FIG. 2: Posterior samples from joint re-analysis of one of the mock doubly lensed GW events detected by LVK O5 network using `nessai` nested sampling in `Bilby`. The estimated parameters include chirp mass  $\mathcal{M}_c [M_\odot]$ , mass ratio  $q$ , GW luminosity distance  $d_L^{\text{GW}} [\text{Gpc}]$ , inclination angle  $\iota$ , and impact parameter  $y$ . The orange lines show the injected values for parameters.

`scipy.gaussian_kde` under Scott's Rule. Then we compute the average posterior PDF over all  $N_{\text{real}}$  realizations by<sup>12</sup>

$$P_{\text{avg}}(\lambda|x) = \frac{1}{N_{\text{real}}} \sum_{i=1}^{N_{\text{real}}} P_i(\lambda|x). \quad (5.1)$$

We perform the inference in four different cosmology models, namely the  $\Lambda$ CDM model, the  $w_0 w_a$ CDM model, the  $(\Xi_0, n)$  modified gravity model, and the  $\alpha$ -basis scalar-tensor gravity model. The inference results are presented in the following subsections.

### A. $\Lambda$ CDM model

For the  $\Lambda$ CDM model, we estimate  $H_0$  and  $\Omega_{m,0}$ , while assuming  $\Omega_{\Lambda,0} = 1 - \Omega_{m,0}$  in the late universe. The averaged posteriors over all realizations are shown in Figure 3. We see that for the LVK O5 network and the post-O5 network, the constraints on  $H_0$  and  $\Omega_{m,0}$  are weak, which is due to the limited number of lensed events. The

<sup>12</sup> Realizations with no qualified lensed events are not included in averaging.

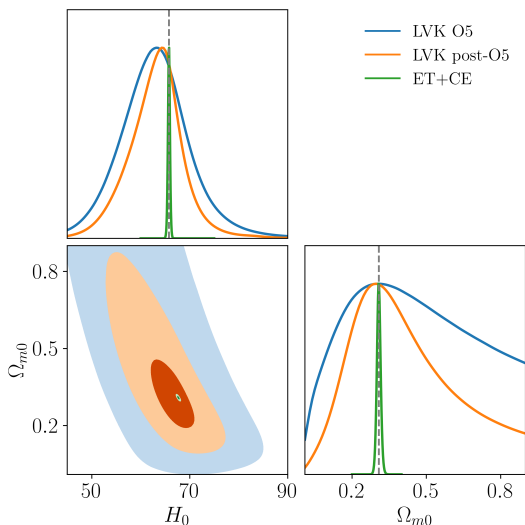


FIG. 3: The figure shows the forecasted posterior on cosmological parameters in the  $\Lambda$ CDM model by jointly analyzing all lensed GW events in each realization, and averaging over all realizations, with different detector networks. The grey dashed lines indicate the parameter values in the fiducial  $\Lambda$ CDM model.

relative  $1\sigma$  uncertainty of  $H_0$  is around 14% and 10% for the O5 and the post-O5 network respectively (See exact number in Table I). For  $\Omega_{m,0}$ , the relative  $1\sigma$  uncertainty reaches 100% and 73% respectively. However, for the ET+CE network, the cosmological constraints are greatly improved, because the lensed event number is over 1 orders of magnitude larger than the LVK network, and the event SNRs are much larger. The relative  $1\sigma$  uncertainties on  $H_0$  and  $\Omega_{m,0}$  for the ET+CE network reduce to around 0.42% and 2.6% respectively. Such precision is comparable to Planck’s measurement and other local-universe measurements, making doubly lensed GWs + strong lensing galaxy survey an accurate independent probe of  $H_0$  that could provide a new insight to the Hubble tension.

### B. $w_0w_a$ CDM model

In the dynamical dark energy model with the CPL parameterization, we estimate  $H_0$ ,  $\Omega_{m,0}$ ,  $w_0$ , and  $w_a$ , based on modification in  $d_L^{\text{GW}}$  with equation (2.14). As shown by averaged posteriors over all realizations in Figure 4,  $w_0$  and  $w_a$  are basically unconstrained with the LVK O5 and post-O5 network. On one hand, there are too few lensed events that can be associated with galaxy surveys for LVK sensitivity. On the other hand, the redshift range of LVK events are mostly at  $z \lesssim 2$ , while precise constraints on  $w_0$  and  $w_a$  rely on high-redshift events. For the ET+CE network, we can see moderate constraints on  $w_0$  and  $w_a$ , with uncertainties of  $\sim 0.3$  for  $w_0$ , and around order of unity for  $w_a$ . It demonstrates the potential of doubly lensed GW events to constrain dynamical

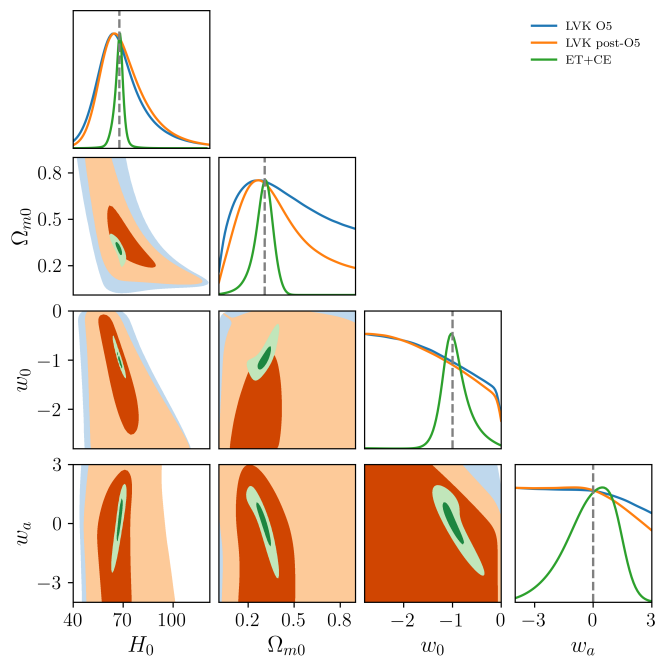


FIG. 4: The figure shows the forecasted posterior on cosmological parameters in the  $w_0w_a$ CDM model by jointly analyzing all lensed GW events in each realization, and averaging over all realizations, with different detector networks. The grey dashed lines indicate the parameter values in the fiducial  $\Lambda$ CDM model.

dark energy in the near future. If the observation period of ET+CE can last longer, the uncertainty on  $w_0$  and  $w_a$  can be further reduced, making our method competitive to other EM probes.

In addition, constraints on  $H_0$  and  $\Omega_{m,0}$  in the  $w_0w_a$ CDM model are also weakened compared to the  $\Lambda$ CDM model. The relative  $1\sigma$  uncertainty on  $H_0$  becomes 21% for both the LVK O5 and post-O5 network, and 3.9% for the ET+CE network, which is increased by  $\sim 8.3$  times. The evolution of the precision on  $H_0$  measurement by different detector networks is shown in Figure 5. However, the uncertainty on  $\Omega_{m,0}$  only increases slightly for the LVK O5 and post-O5 network, which may be due to the fact that  $\Omega_{m,0}$  is already poorly constrained by LVK. But it has climbed to 19% for the ET+CE network, which is  $\sim 7.3$  times the  $\Omega_{m,0}$  uncertainty in the  $\Lambda$ CDM model. precision

### C. $(\Xi_0, n)$ modified gravity model

We also analyze the constraints on modified gravity models with our method. For the  $(\Xi_0, n)$  parameterization, we jointly estimate  $H_0$ ,  $\Omega_{m,0}$ ,  $\Xi_0$  and  $n$ . The averaged posteriors over all realizations are presented in Figure 6. For the LVK network, we obtain moderate constraints on  $H_0$  and  $\Xi_0$ , with a relative uncertainty in

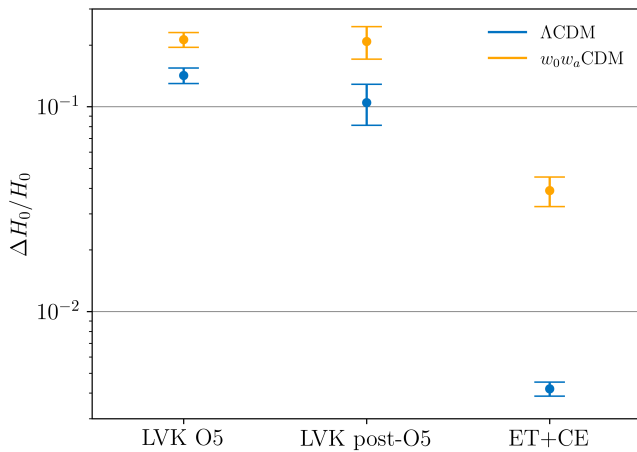


FIG. 5: Fractional  $1\sigma$  uncertainty of  $H_0$  in the  $\Lambda$ CDM model (blue) and  $w_0w_a$ CDM model (orange) with different detector networks. The upper and lower bars show the upper and lower  $1\sigma$  uncertainty bounds respectively, and the circles represent their means.

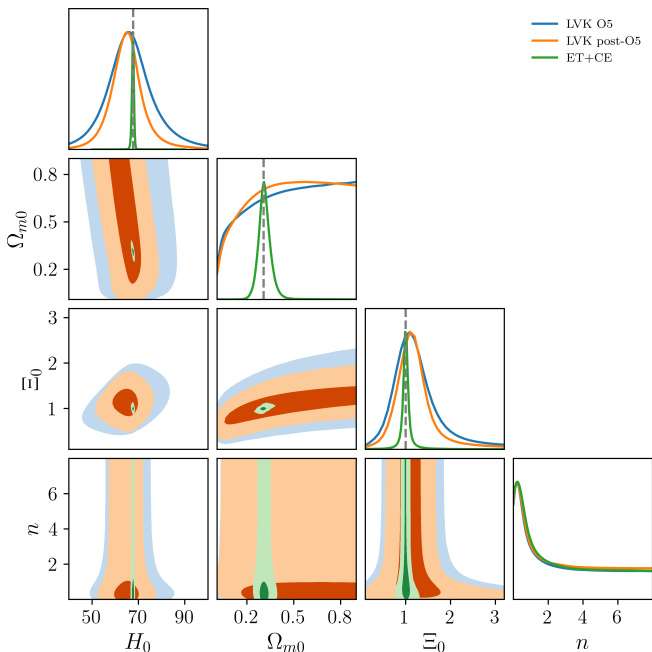


FIG. 6: The figure shows the forecasted posterior on cosmological parameters in the  $(\Xi_0, n)$  modified gravity model by jointly analyzing all lensed GW events in each realization, and averaging over all realizations, with different detector networks. The grey dashed lines indicate the parameter values in the fiducial  $\Lambda$ CDM model.

$H_0$  of 15% and 10% for the O5 network and the post-O5 network respectively, which is comparable to the  $\Lambda$ CDM case. But the relative uncertainty in  $\Xi_0$  is 49% and 35% for the O5 network and the post-O5 network respectively. The constraint on  $\Xi_0$  is not as tight as that on  $H_0$ , be-

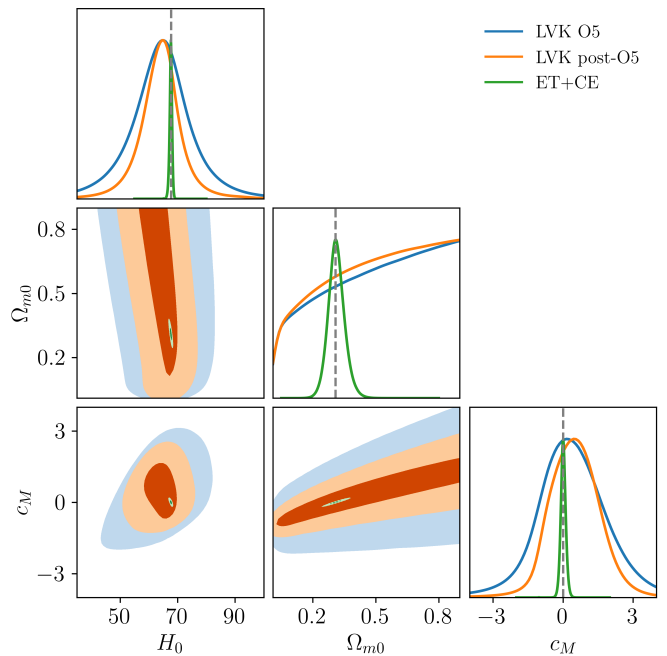


FIG. 7: The figure shows the forecasted posterior on cosmological parameters in the scalar-tensor gravity model by jointly analyzing all lensed GW events in each realization, and averaging over all realizations, with different detector networks. The grey dashed lines indicate the parameter values in the fiducial  $\Lambda$ CDM model.

cause  $\Xi_0$  only modifies  $d_L^{\text{GW}}$  via equation (2.17) in the GW waveform, but not the angular diameter distances in lens systems from EM probes, while  $H_0$  affects all these distances. However, we obtain poor constraints on  $\Omega_{m,0}$  for the LVK network, probably due to its degeneracy with  $H_0$  and  $\Xi_0$ . On the other hand, with the ET+CE network, we obtain strong constraints on  $H_0$  and  $\Xi_0$ , and moderate constraint on  $\Omega_{m,0}$ . The relative uncertainties are 0.7% and 7.9% for  $H_0$  and  $\Xi_0$ , and 12% for  $\Omega_{m,0}$ . Finally, we find that the constraints on  $n$  favor a value near the lower bound, but they are not converged at the higher bound, for all of the detector networks. It could be explained by the fact that the fiducial  $\Lambda$ CDM case corresponds to either  $n = 0$ , or any value of  $n$  for  $\Xi_0 = 1$ .

#### D. $\alpha$ -basis modified gravity model

Apart from the general  $(\Xi_0, n)$  modified gravity parametrization, we estimate constraints on the  $\alpha$ -basis parametrization as well. Here,  $d_L^{\text{GW}}$  is modified by equation (2.18), so we jointly estimate  $H_0$ ,  $\Omega_{m,0}$  and  $c_M$ . As shown by the averaged posteriors over all realizations in Figure 7, the constraints on  $H_0$ ,  $\Omega_{m,0}$  and  $c_M$  are similar to those on  $H_0$ ,  $\Omega_{m,0}$  and  $\Xi_0$  in the  $(\Xi_0, n)$  parameterization. The relative uncertainty on  $H_0$  is 16%, 10%, and 0.6% for the LVK O5, post-O5, and ET+CE network,

		LVK O5	LVK post-O5	ET+CE
$\Lambda$ CDM	$H_0$	$64.40^{+8.36}_{-9.97}$	$65.91^{+5.34}_{-8.48}$	$67.70^{+0.31}_{-0.26}$
	$\Omega_{m,0}$	$0.306^{+0.391}_{-0.187}$	$0.296^{+0.279}_{-0.147}$	$0.308^{+0.009}_{-0.007}$
$w_0 w_a$ CDM	$H_0$	$64.16^{+14.77}_{-12.51}$	$64.68^{+15.92}_{-11.04}$	$68.01^{+2.22}_{-3.09}$
	$\Omega_{m,0}$	$0.271^{+0.392}_{-0.191}$	$0.267^{+0.274}_{-0.177}$	$0.313^{+0.056}_{-0.065}$
	$w_0$	-	-	$-1.02^{+0.31}_{-0.22}$
	$w_a$	-	-	$0.48^{+0.99}_{-1.54}$
$(\Xi_0, n)$	$H_0$	$65.92^{+9.89}_{-10.34}$	$65.25^{+6.24}_{-7.26}$	$67.69^{+0.40}_{-0.52}$
	$\Omega_{m,0}$	-	$0.559^{+0.381}_{-0.233}$	$0.310^{+0.040}_{-0.035}$
	$\Xi_0$	$1.08^{+0.57}_{-0.48}$	$1.13^{+0.38}_{-0.42}$	$1.003^{+0.076}_{-0.082}$
	$n$	$0.21^{+6.46}_{-0.21}$	$0.21^{+6.63}_{-0.21}$	$0.36^{+6.31}_{-0.36}$
$\alpha$ -basis	$H_0$	$64.86^{+10.02}_{-10.79}$	$64.88^{+5.85}_{-7.49}$	$67.69^{+0.37}_{-0.48}$
	$\Omega_{m,0}$	-	-	$0.309^{+0.040}_{-0.036}$
	$c_M$	$0.17^{+1.59}_{-1.28}$	$0.48^{+0.97}_{-1.10}$	$0.006^{+0.104}_{-0.107}$

TABLE I: Cosmological parameter constraints with  $1\sigma$  uncertainty in different models from marginalized posteriors averaged over all realizations.

respectively.  $\Omega_{m,0}$  is again unconstrained with the LVK network, but is moderately constrained with a relative error of 12% for the ET+CE network. For  $c_M$ , the fiducial value in the  $\Lambda$ CDM model is  $c_M = 0$ . The mean uncertainty of the upper bound and the lower bound of  $c_M$  is 1.44, 1.04, and 0.106, for the LVK O5, post-O5, and the ET+CE network, respectively. Similar to the degeneracy between  $\Omega_{m,0}$  and  $\Xi_0$  in the  $(\Xi_0, n)$  model, we can also see degeneracy between  $\Omega_{m,0}$  and  $c_M$ , but it is a bit stronger. This is likely because  $d_L^{\text{GW}}/d_L^{\text{EM}}$  depends on both  $\Omega_{m,0}$  and  $c_M$  in the  $\alpha$ -basis model, while it is independent of  $\Omega_{m,0}$  in the  $(\Xi_0, n)$  model.

## VI. CONCLUSION

In this work, we generalize GW lensing cosmography by associating doubly lensed GWs with strong lensing systems in galaxy surveys. By jointly re-analyzing the two lensed GW images using the SIS lens model, we can measure  $d_L^{\text{GW}}$  for the unlensed waveform and the impact parameter  $y$ . Under precise lensed GW localization with the effective detector network, the lens galaxy and the host galaxy of lensed GWs are very likely to be identified from strong lensing catalogues, which could provide redshift of the lens and the source, as well as Einstein radius in the SIS model from the two image positions. With these observables, we can constrain cosmological parameters and modified GW propagation effects by combining time-delay cosmography and the standard siren approach. We simulate lensed GWs from BBH mergers detected by the LVK O5/post-O5 network and the ET+CE network, and select events within the range and resolvability by the LSST.

By simulating 1000 realizations, we find that the chance to observe lensed GWs by the LVK O5 network that can be associated with LSST is low, with an aver-

age detection number of 0.2. But once such events are detected, they are expected to provide moderate constraints on  $H_0$  with 14% uncertainty and modified GW propagation effects. With the LVK post-O5 network, the average detection number of lensed GWs associated with LSST increases to 2.4, which slightly enhance the cosmological constraints, but dynamical dark energy remains unconstrained. However, using the ET+CE network, we can detect an average of 73.2 lensed GWs associated with LSST over 100 realizations. They can provide strong constraint on  $H_0$  with 0.42% uncertainty and on  $\Omega_{m,0}$  with 2.6% uncertainty in the  $\Lambda$ CDM model. It can also provide moderate constraint on  $w_0$  and  $w_a$  in the  $w_0 w_a$  CDM model for dynamical dark energy, yielding  $w_0 = -1.02^{+0.31}_{-0.22}$  and  $w_a = 0.48^{+0.99}_{-1.54}$ . It demonstrates the potential of our method to give an independent measurement of  $H_0$  and shed light on the Hubble tension problem. Furthermore, it could also jointly constrain modified GW propagation effects with a high precision.

As discussed in literature, a small portion of strongly lensed GWs can produce more than two images. For triply lensed or quadruply lensed GWs, one can reconstruct the lens system with a more comprehensive lens model, such as the singular isothermal ellipsoid (SIE) model, using software like `lenstronomy` [96]. With 10 quadruply lensed GWs detected by ET+CE and the images of their lensing systems, one can also constrain  $H_0$  with an uncertainty  $< 1\%$  [21]. Although the constraint by a single doubly lensed event is less accurate than a quadruply lensed event due to the difficulty in reconstructing the Fermat potential, the combination of a larger number of doubly lensed events can still provide a competitive constraint. However, the identification and localization of doubly lensed events would be more challenging than quadruply lensed events, especially for the LVK network when the GW sky localization is not sufficiently precise. The detectability of lensed events also depends on accurate matching between lensed signals, careful lens model selection [97], and accounting for the selection effects of lensed signals. Nevertheless, a combination of doubly lensed GWs and quadruply lensed GWs will further enhance the cosmological constraints.

Apart from direct constraints from strongly lensed GWs and their EM counterparts in galaxy catalogues, there are other proposals to constrain cosmology and modified gravity using lensed GWs as well, for example, using lensed GW population and time-delay distribution [98–101], or cross-correlation between weak-lensing of GWs and galaxy surveys [102, 103]. These independent methods could further provide great complements to the cosmological constraints with GW lensing. In conclusion, with the promising future of next-generation GW detectors and large scale galaxy surveys, GW lensing cosmography will be a powerful tool in the era of precision cosmology.

## ACKNOWLEDGMENTS

We thank Eungwang Seo for insightful comments during the internal review of our manuscript. A.C. is supported by the China Postdoctoral Science Foundation under Grant No. 2025M773325, and the National Natural Science Foundation of China (NSFC) under Grant No. E414660101 and 12147103. J.Z. is supported by the NSFC under Grants No. E414660101 and No. 12147103, and the Fundamental Research Funds for the Central Universities under Grants No. E4EQ6604X2 and No. E3ER6601A2. This material is based upon work supported by NSF’s LIGO Laboratory which is a major facility fully funded by the National Science Foundation. We are grateful to the High Performance Computing Center (HPCC) of ICTP-AP for performing the numerical computations in this paper.

## Appendix A: GW population model

In our work, we simulate mock BBH events with a population model in the space of mass and redshift given by

$$p_{\text{pop}}(m_1^s, m_2^s, z | \Lambda_m, \Lambda_r) \propto p(m_1^s, m_2^s | \Lambda_m) p_{\text{rate}}(z | \Lambda_r) \frac{dV_c}{dz}, \quad (\text{A1})$$

where  $m_1^s, m_2^s$  are the source-frame mass.  $dV_c/dz$  is the differential comoving volume. We adopt the Power-law + Double Peak black hole mass distribution model, which is a phenomenological model well fitted by GWTC-4 data [12]. It is described by 10 parameters: minimal mass  $M_{\text{min}}$ , maximal mass  $M_{\text{max}}$ , slope of the power-law component of the primary mass distribution  $\alpha$ , fraction of both Gaussian components in the primary mass distribution,  $\lambda_g$ , fraction of the lower Gaussian component in the two Gaussian components  $\lambda_{g,\text{low}}$ , mean of the lower and higher Gaussian component of the primary mass distribution  $\mu_{g,\text{low}}, \mu_{g,\text{high}}$ , width of the lower and higher Gaussian component of the primary mass distribution,  $\sigma_{g,\text{low}}, \sigma_{g,\text{high}}$ , and the range of mass tapering at the lower end of the mass distribution  $\delta_m$ . The primary mass prior for this population model is given by

$$p(m_1^s | \Lambda_m) = (1 - \lambda_g) \mathcal{B}(m_1^s | M_{\text{min}}, M_{\text{max}}, \alpha) + \lambda_g \lambda_{g,\text{low}} \mathcal{G}(m_1^s | \mu_{g,\text{low}}, \sigma_{g,\text{low}}) + \lambda_g (1 - \lambda_{g,\text{low}}) \mathcal{G}(m_1^s | \mu_{g,\text{high}}, \sigma_{g,\text{high}}), \quad (\text{A2})$$

where  $\mathcal{B}$  represents the broken power-law distribution, and  $\mathcal{G}$  is the Gaussian distribution. The secondary mass is then drawn with a power-law mass ratio distribution with a slope of  $\beta$ .

We also apply the Madau-Dickinson merger rate redshift evolution model inspired from the Madau-Dickinson star formation rate [104] to our simulation, which is used by the GWTC-4 cosmology paper [12]. The merger rate

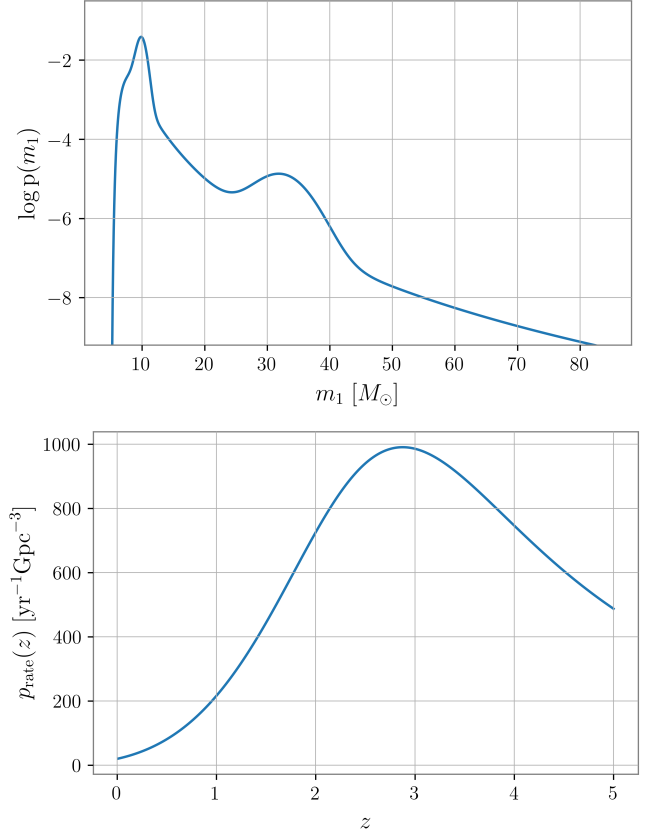


FIG. 8: Upper panel: Powerlaw + Double Peak black hole mass distribution model. Lower panel: Madau-Dickinson merger-rate redshift evolution model. Both figures are plotted with the parameter values from GWTC-4 cosmology analysis [12].

in function of redshift is given by

$$p_{\text{rate}}(z | \Lambda_r) = R_0 [1 + (1 + z_p)^{-\gamma - k}] \frac{(1 + z)^\gamma}{1 + \left(\frac{1 + z}{1 + z_p}\right)^{\gamma + k}}, \quad (\text{A3})$$

where  $R_0$  is the merger rate at  $z = 0$ ,  $\gamma$  and  $k$  are the slopes of the powerlaw rate evolution at redshift lower and higher than the turning point  $z_p$ , respectively. In our simulation, we adopt the parameter values from GWTC-4 cosmology analysis [12], which are  $M_{\text{min}} = 4.72 M_\odot$ ,  $M_{\text{max}} = 84.28 M_\odot$ ,  $\alpha = 2.97$ ,  $\beta = 0.83$ ,  $\mu_{g,\text{low}} = 9.91 M_\odot$ ,  $\sigma_{g,\text{low}} = 0.83 M_\odot$ ,  $\lambda_{g,\text{low}} = 0.86$ ,  $\mu_{g,\text{high}} = 32.31 M_\odot$ ,  $\sigma_{g,\text{high}} = 4.24 M_\odot$ ,  $\lambda_{g,\text{high}} = 0.28$ ,  $\delta_m = 4.71 M_\odot$ ,  $\gamma = 3.46$ ,  $k = 2.90$ , and  $z_p = 2.77$ . For the merger rate today, we adopt a typical value  $R_0 = 20 \text{yr}^{-1} \text{Gpc}^{-3}$ . The corresponding mass distribution and redshift evolution are plotted in Figure 8.

## Appendix B: Optical depth of sources

The probability of a background source to be lensed by a foreground galaxy is also known as the optical depth. Its differentiation with respect to the redshift and the velocity dispersion of the lens galaxy is give by [18]

$$\frac{d^2\tau}{dz_L d\sigma} = \frac{dn}{d\sigma}(z_L, \sigma) s_{\text{cr}}(z_L, \sigma) \frac{cdt}{dz_L}(z_L), \quad (\text{B1})$$

where  $s_{\text{cr}}$  is the cross section of the signal deflection in the lens system. The lens number density distribution with respect to the galaxy velocity dispersion  $\sigma$  can be modelled by a modified Schechter function [105] as

$$\frac{dn}{d\sigma} = n_* \left( \frac{\sigma}{\sigma_*} \right)^\alpha \exp \left[ - \left( \frac{\sigma}{\sigma_*} \right)^\beta \right] \frac{\beta}{\Gamma[\alpha/\beta]} \frac{1}{\sigma}, \quad (\text{B2})$$

where  $\alpha$  is the faint-end slope,  $\beta$  is the high-velocity cut-off, and  $n_*$  and  $\sigma_*$  are the characteristic number density and velocity dispersion, which could be parameterized in a form evolving with redshift as  $n_*(z) = n_{*,0}(1+z)^{3-\nu_{n^*}}$  and  $\sigma_*(z) = \sigma_{*,0}(1+z)^{\nu_{\sigma^*}}$ . In our work, we adopt the constant comoving lens number density, so that  $\nu_{n^*} = \nu_{\sigma^*} = 0$ .

The lensing statistic in a finite transient observation needs to account for the missing events due to the time delay of lensed signals [106]. The SIS cross section in a transient survey is given by

$$s_{\text{cr}}(z_L, \sigma) = \pi D_L^2 \theta_E^2 \int_{y_{\text{min}}}^{y_{\text{max}}} f(\Delta t(y; \sigma, z_L)) y dy, \quad (\text{B3})$$

where  $f(\Delta t)$  is the fraction of lensed events with time delay  $\Delta t$  that can be observed. Assuming a uniform distribution of lensed signal arrival time during the continuous transient observation time  $T_{\text{obs}}$ , we have

$$f(\Delta t) = 1 - \frac{\Delta t}{T_{\text{obs}}} \quad (\text{B4})$$

for  $\Delta t < T_{\text{obs}}$ , and  $f(\Delta t) = 0$  otherwise. Then the cross section in equation (B3) results in

$$s_{\text{cr}} = \pi D_L^2 \theta_E^2 \left[ (y_{\text{max}}^2 - y_{\text{min}}^2) - \frac{2}{3} \frac{\Delta t_z}{T_{\text{obs}}} (y_{\text{max}}^3 - y_{\text{min}}^3) \right]. \quad (\text{B5})$$

For the SIS model, we have  $y_{\text{min}} = 0$ . By inserting the above equation into equation (B1) and integrating it over  $\sigma$  in  $(0, \infty)$ , we arrive at

$$\tau = \frac{F_*}{30} [D_S(1+z_S)]^3 y_{\text{max}}^2 \left\{ 1 - \frac{1}{7} \frac{\Gamma[(8+\alpha)/\beta]}{\Gamma[(4+\alpha)/\beta]} \frac{\Delta t_*}{T_{\text{obs}}} \right\}, \quad (\text{B6})$$

where

$$F_* = 16\pi^3 n_{*,0} \left( \frac{\sigma_{*,0}}{c} \right)^4 \frac{\Gamma[(4+\alpha)/\beta]}{\Gamma[\alpha/\beta]}, \quad (\text{B7})$$

$$\Delta t_* = 32\pi^2 \left( \frac{\sigma_{*,0}}{c} \right)^4 \frac{D_S}{c} (1+z_S) y_{\text{max}}, \quad (\text{B8})$$

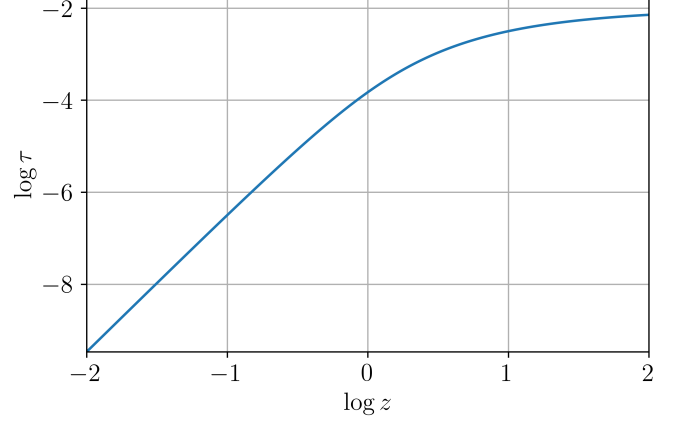


FIG. 9: Optical depth of background sources computed with equation (B6) using  $n_{*,0} = 8.0 \times 10^{-3} h^3 \text{Mpc}^{-3}$ ,  $\sigma_{*,0} = 144 \text{ km s}^{-1}$ ,  $\alpha = 2.49$ , and  $\beta = 2.29$ .

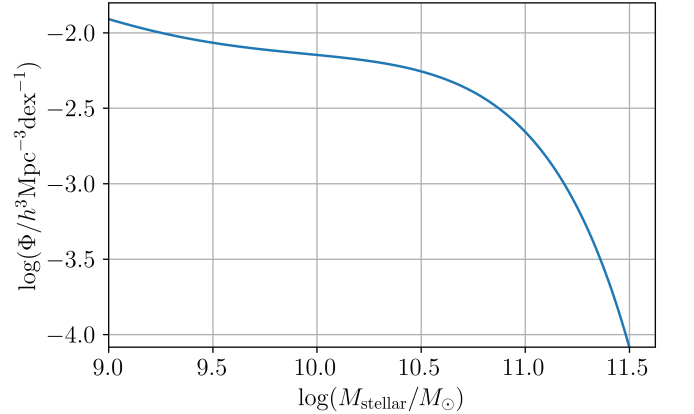


FIG. 10: The density profile of lens galaxies in stellar masses computed with equation (4.5).

Figure 9 shows the optical depth computed with parameters used in Section IV B. In addition, 10 shows the density profile of lens galaxies in stellar masses described by the double Schechter function in equation (4.5).

[1] M. Abdul Karim *et al.* (DESI), DESI DR2 results. II. Measurements of baryon acoustic oscillations and cos-

mological constraints, Phys. Rev. D **112**, 083515 (2025),

- arXiv:2503.14738 [astro-ph.CO].
- [2] G. Gu *et al.* (DESI), Dynamical Dark Energy in light of the DESI DR2 Baryonic Acoustic Oscillations Measurements, *Nature Astronomy* 10.1038/s41550-025-02669-6 (2025), arXiv:2504.06118 [astro-ph.CO].
  - [3] N. Aghanim *et al.* (Planck), Planck 2018 results. VI. Cosmological parameters, *Astron. Astrophys.* **641**, A6 (2020), [Erratum: *Astron. Astrophys.* 652, C4 (2021)], arXiv:1807.06209 [astro-ph.CO].
  - [4] A. G. Riess, S. Casertano, W. Yuan, L. M. Macri, and D. Scolnic, Large Magellanic Cloud Cepheid Standards Provide a 1% Foundation for the Determination of the Hubble Constant and Stronger Evidence for Physics beyond  $\Lambda$ CDM, *Astrophys. J.* **876**, 85 (2019), arXiv:1903.07603 [astro-ph.CO].
  - [5] E. Abdalla *et al.*, Cosmology intertwined: A review of the particle physics, astrophysics, and cosmology associated with the cosmological tensions and anomalies, *JHEAp* **34**, 49 (2022), arXiv:2203.06142 [astro-ph.CO].
  - [6] A. G. Abac *et al.* (LIGO Scientific, VIRGO, KAGRA), GWTC-4.0: Updating the Gravitational-Wave Transient Catalog with Observations from the First Part of the Fourth LIGO-Virgo-KAGRA Observing Run, (2025), arXiv:2508.18082 [gr-qc].
  - [7] B. Schutz, Determining the hubble constant from gravitational wave observations, *Nature* **323**, 310 (1986).
  - [8] B. P. Abbott *et al.* (LIGO Scientific, Virgo, 1M2H, Dark Energy Camera GW-E, DES, DLT40, Las Cumbres Observatory, VINROUGE, MASTER), A gravitational-wave standard siren measurement of the Hubble constant, *Nature* **551**, 85 (2017), arXiv:1710.05835 [astro-ph.CO].
  - [9] R. Abbott *et al.* (LIGO Scientific, Virgo, KAGRA), Constraints on the Cosmic Expansion History from GWTC-3, *Astrophys. J.* **949**, 76 (2023), arXiv:2111.03604 [astro-ph.CO].
  - [10] S. Mastroianni, D. Laghi, R. Gray, G. C. Santoro, A. Ghosh, C. Karathanasis, K. Leyde, D. A. Steer, S. Perries, and G. Pierra, Joint population and cosmological properties inference with gravitational waves standard sirens and galaxy surveys, *Phys. Rev. D* **108**, 042002 (2023), arXiv:2305.10488 [astro-ph.CO].
  - [11] R. Gray *et al.*, Joint cosmological and gravitational-wave population inference using dark sirens and galaxy catalogues, *JCAP* **12**, 023, arXiv:2308.02281 [astro-ph.CO].
  - [12] A. G. Abac *et al.* (LIGO Scientific, VIRGO, KAGRA), GWTC-4.0: Constraints on the Cosmic Expansion Rate and Modified Gravitational-wave Propagation, arXiv:2509.04348 (2025), arXiv:2509.04348 [astro-ph.CO].
  - [13] S.-J. Jin, J.-Y. Song, T.-Y. Sun, S.-R. Xiao, H. Wang, L.-F. Wang, J.-F. Zhang, and X. Zhang, Gravitational wave standard sirens: A brief review of cosmological parameter estimation, *Sci. China Phys. Mech. Astron.* **69**, 220401 (2026), arXiv:2507.12965 [astro-ph.CO].
  - [14] M. Branchesi *et al.*, Science with the Einstein Telescope: a comparison of different designs, *J. Cosmol. Astropart. Phys.* **07**, 068, arXiv:2303.15923 [gr-qc].
  - [15] M. Evans *et al.*, A Horizon Study for Cosmic Explorer: Science, Observatories, and Community, (2021), arXiv:2109.09882 [astro-ph.IM].
  - [16] H.-Y. Chen, J. M. Ezquiaga, and I. Gupta, Cosmography with next-generation gravitational wave detectors, *Class. Quant. Grav.* **41**, 125004 (2024), arXiv:2402.03120 [gr-qc].
  - [17] A. Chen, Measuring the cosmic dipole with golden dark sirens in the era of next-generation ground-based gravitational wave detectors, *JCAP* **07**, 076, arXiv:2505.12678 [gr-qc].
  - [18] M. Sereno, P. Jetzer, A. Sesana, and M. Volonteri, Cosmography with strong lensing of LISA gravitational wave sources, *Mon. Not. Roy. Astron. Soc.* **415**, 2773 (2011), arXiv:1104.1977 [astro-ph.CO].
  - [19] O. A. Hannuksela, T. E. Collett, M. Çalıřkan, and T. G. F. Li, Localizing merging black holes with sub-arcsecond precision using gravitational-wave lensing, *Mon. Not. Roy. Astron. Soc.* **498**, 3395 (2020), arXiv:2004.13811 [astro-ph.HE].
  - [20] S.-J. Huang, Y.-M. Hu, X. Chen, J.-d. Zhang, E.-K. Li, Z. Gao, and X.-Y. Lin, Measuring the Hubble constant using strongly lensed gravitational wave signals, *JCAP* **08**, 003, arXiv:2304.10435 [astro-ph.CO].
  - [21] Z. Chen, Q. Yu, Y. Lu, and X. Guo, Enhanced Localization of Dark Lensed Gravitational Wave Events Enables Host Galaxy Identification and Precise Cosmological Inference, (2025), arXiv:2510.12470 [astro-ph.CO].
  - [22] S. Refsdal, On the Possibility of Determining Hubble's Parameter and the Masses of Galaxies from the Gravitational Lens Effect, *Mon. Not. Roy. Astron. Soc.* **128**, 307 (1964).
  - [23] T. Treu and P. J. Marshall, Time Delay Cosmography, *Astron. Astrophys. Rev.* **24**, 11 (2016), arXiv:1605.05333 [astro-ph.CO].
  - [24] K. C. Wong *et al.* (H0LiCOW), H0LiCOW – XIII. A 2.4 per cent measurement of H0 from lensed quasars: 5.3 $\sigma$  tension between early- and late-Universe probes, *Mon. Not. Roy. Astron. Soc.* **498**, 1420 (2020), arXiv:1907.04869 [astro-ph.CO].
  - [25] S. Birrer *et al.*, TDCOSMO - IV. Hierarchical time-delay cosmography – joint inference of the Hubble constant and galaxy density profiles, *Astron. Astrophys.* **643**, A165 (2020), arXiv:2007.02941 [astro-ph.CO].
  - [26] S. Birrer, M. Millon, D. Sluse, A. J. Shajib, F. Courbin, S. Erickson, L. V. E. Koopmans, S. H. Suyu, and T. Treu, Time-Delay Cosmography: Measuring the Hubble Constant and Other Cosmological Parameters with Strong Gravitational Lensing, *Space Sci. Rev.* **220**, 48 (2024), arXiv:2210.10833 [astro-ph.CO].
  - [27] S. H. Suyu, A. Goobar, T. Collett, A. More, and G. Varnardos, Strong Gravitational Lensing and Microlensing of Supernovae, *Space Sci. Rev.* **220**, 13 (2024), arXiv:2301.07729 [astro-ph.CO].
  - [28] S. Birrer *et al.* (TDCOSMO), TDCOSMO 2025: Cosmological constraints from strong lensing time delays, in *3rd General Meeting of CosmoVerse: Addressing observational tensions in cosmology with systematics and fundamental physics* (2025) arXiv:2506.03023 [astro-ph.CO].
  - [29] K. Liao, X.-L. Fan, X.-H. Ding, M. Biesiada, and Z.-H. Zhu, Precision cosmology from future lensed gravitational wave and electromagnetic signals, *Nature Commun.* **8**, 1148 (2017), [Erratum: *Nature Commun.* **8**, 2136 (2017)], arXiv:1703.04151 [astro-ph.CO].
  - [30] S.-S. Li, S. Mao, Y. Zhao, and Y. Lu, Gravitational lensing of gravitational waves: A statistical perspective, *Mon. Not. Roy. Astron. Soc.* **476**, 2220 (2018), arXiv:1802.05089 [astro-ph.CO].

- [31] N. Lines *et al.*, Euclid quick data release (q1). the strong lensing discovery engine c: Finding lenses with machine learning, *Astron. Astrophys.* 10.1051/0004-6361/202554542 (2025).
- [32] A. J. Shajib†, G. P. Smith, S. Birrer, A. Verma, N. Arendse, T. E. Collett, T. Daylan, and S. Serjeant (LSST Strong Lensing Science), Strong gravitational lenses from the Vera C. Rubin Observatory, *Phil. Trans. Roy. Soc. Lond. A* **383**, 20240117 (2025), arXiv:2406.08919 [astro-ph.CO].
- [33] E. Belgacem, Y. Dirian, S. Foffa, and M. Maggiore, Modified gravitational-wave propagation and standard sirens, *Phys. Rev. D* **98**, 023510 (2018), arXiv:1805.08731 [gr-qc].
- [34] E. Belgacem *et al.* (LISA Cosmology Working Group), Testing modified gravity at cosmological distances with LISA standard sirens, *JCAP* **07**, 024, arXiv:1906.01593 [astro-ph.CO].
- [35] M. Lagos, M. Fishbach, P. Landry, and D. E. Holz, Standard sirens with a running Planck mass, *Phys. Rev. D* **99**, 083504 (2019), arXiv:1901.03321 [astro-ph.CO].
- [36] S. Mukherjee, B. D. Wandelt, and J. Silk, Testing the general theory of relativity using gravitational wave propagation from dark standard sirens, *Mon. Not. Roy. Astron. Soc.* **502**, 1136 (2021), arXiv:2012.15316 [astro-ph.CO].
- [37] A. Finke, S. Foffa, F. Iacovelli, M. Maggiore, and M. Mancarella, Cosmology with LIGO/Virgo dark sirens: Hubble parameter and modified gravitational wave propagation, *JCAP* **08**, 026, arXiv:2101.12660 [astro-ph.CO].
- [38] K. Leyde, S. Mastrogiovanni, D. A. Steer, E. Chassande-Mottin, and C. Karathanasis, Current and future constraints on cosmology and modified gravitational wave friction from binary black holes, *JCAP* **09**, 012, arXiv:2202.00025 [gr-qc].
- [39] A. Chen, R. Gray, and T. Baker, Testing the nature of gravitational wave propagation using dark sirens and galaxy catalogues, *JCAP* **02**, 035, arXiv:2309.03833 [gr-qc].
- [40] C. Lin, T. Zhu, R. Niu, and W. Zhao, Constraining the modified friction in gravitational wave propagation with precessing black hole binaries, *Phys. Rev. D* **112**, 024010 (2025), arXiv:2404.11245 [gr-qc].
- [41] D. Maoz and H.-W. Rix, Early type galaxies, dark halos, and gravitational lensing statistics, *Astrophys. J.* **416**, 425 (1993).
- [42] C. S. Kochanek, Is there a cosmological constant?, *Astrophys. J.* **466**, 638 (1996), arXiv:astro-ph/9510077.
- [43] J. L. Mitchell, C. R. Keeton, J. A. Frieman, and R. K. Sheth, Robust cosmological constraints from gravitational lens statistics, *Astrophys. J.* **622**, 81 (2005), arXiv:astro-ph/0401138.
- [44] J. Binney and S. Tremaine, *Galactic dynamics* (1987).
- [45] R. Takahashi and T. Nakamura, Wave effects in the gravitational lensing of gravitational waves from chirping binaries, *The Astrophysical Journal* **595**, 1039 (2003).
- [46] R. Takahashi, Arrival time differences between gravitational waves and electromagnetic signals due to gravitational lensing, *Astrophys. J.* **835**, 103 (2017), arXiv:1606.00458 [astro-ph.CO].
- [47] J. M. Ezquiaga, D. E. Holz, W. Hu, M. Lagos, and R. M. Wald, Phase effects from strong gravitational lensing of gravitational waves, *Phys. Rev. D* **103**, 064047 (2021), arXiv:2008.12814 [gr-qc].
- [48] C. McIsaac, D. Keitel, T. Collett, I. Harry, S. Mozzon, O. Edy, and D. Bacon, Search for strongly lensed counterpart images of binary black hole mergers in the first two LIGO observing runs, *Phys. Rev. D* **102**, 084031 (2020), arXiv:1912.05389 [gr-qc].
- [49] A. K. Y. Li, R. K. L. Lo, S. Sachdev, J. C. L. Chan, E. T. Lin, T. G. F. Li, and A. J. Weinstein (LIGO Scientific, Virgo), Targeted subthreshold search for strongly lensed gravitational-wave events, *Phys. Rev. D* **107**, 123014 (2023), arXiv:1904.06020 [gr-qc].
- [50] R. Abbott *et al.* (LIGO Scientific, KAGRA, VIRGO), Search for Gravitational-lensing Signatures in the Full Third Observing Run of the LIGO–Virgo Network, *Astrophys. J.* **970**, 191 (2024), arXiv:2304.08393 [gr-qc].
- [51] A. K. Y. Li, J. C. L. Chan, H. Fong, A. H. Y. Chong, A. J. Weinstein, and J. M. Ezquiaga, TESLA-X: An effective method to search for sub-threshold lensed gravitational waves with a targeted population model, *Mon. Not. Roy. Astron. Soc.* **998**, 1010 (2025), arXiv:2311.06416 [gr-qc].
- [52] A. G. Abac *et al.* (LIGO Scientific, VIRGO, KAGRA), GWTC-4.0: Searches for Gravitational-Wave Lensing Signatures, (2025), arXiv:2512.16347 [gr-qc].
- [53] S. Dodelson, *Modern Cosmology* (Academic Press, Amsterdam, 2003).
- [54] M. Chevallier and D. Polarski, Accelerating universes with scaling dark matter, *Int. J. Mod. Phys. D* **10**, 213 (2001), arXiv:gr-qc/0009008.
- [55] E. V. Linder, Exploring the expansion history of the universe, *Phys. Rev. Lett.* **90**, 091301 (2003), arXiv:astro-ph/0208512.
- [56] C. de Rham and S. Melville, Gravitational Rainbows: LIGO and Dark Energy at its Cutoff, *Phys. Rev. Lett.* **121**, 221101 (2018), arXiv:1806.09417 [hep-th].
- [57] T. Baker *et al.* (LISA Cosmology Working Group), Measuring the propagation speed of gravitational waves with LISA, *JCAP* **08** (08), 031, arXiv:2203.00566 [gr-qc].
- [58] T. Baker, E. Barausse, A. Chen, C. de Rham, M. Pieroni, and G. Tassinato, Testing gravitational wave propagation with multiband detections, *JCAP* **03**, 044, arXiv:2209.14398 [gr-qc].
- [59] B. P. Abbott *et al.* (LIGO Scientific, Virgo), GW170817: Observation of Gravitational Waves from a Binary Neutron Star Inspiral, *Phys. Rev. Lett.* **119**, 161101 (2017), arXiv:1710.05832 [gr-qc].
- [60] B. P. Abbott *et al.* (LIGO Scientific, Virgo, Fermi-GBM, INTEGRAL), Gravitational Waves and Gamma-rays from a Binary Neutron Star Merger: GW170817 and GRB 170817A, *Astrophys. J. Lett.* **848**, L13 (2017), arXiv:1710.05834 [astro-ph.HE].
- [61] B. P. Abbott *et al.* (LIGO Scientific, Virgo, Fermi GBM, INTEGRAL, IceCube, AstroSat Cadmium Zinc Telluride Imager Team, IPN, Insight-Hxmt, ANTARES, Swift, AGILE Team, 1M2H Team, Dark Energy Camera GW-EM, DES, DLT40, GRAWITA, Fermi-LAT, ATCA, ASKAP, Las Cumbres Observatory Group, OzGrav, DWF (Deeper Wider Faster Program), AST3, CAASTRO, VINROUGE, MASTER, J-GEM, GROWTH, JAGWAR, CaltechNRAO, TTU-NRAO, NuSTAR, Pan-STARRS, MAXI Team, TZAC Consortium, KU, Nordic Optical Telescope, ePESSTO, GROND, Texas Tech University, SALT

- Group, TOROS, BOOTES, MWA, CALET, IKI-GW Follow-up, H.E.S.S., LOFAR, LWA, HAWC, Pierre Auger, ALMA, Euro VLBI Team, Pi of Sky, Chandra Team at McGill University, DFN, ATLAS Telescopes, High Time Resolution Universe Survey, RIMAS, RATIR, SKA South Africa/MeerKAT), Multi-messenger Observations of a Binary Neutron Star Merger, *Astrophys. J. Lett.* **848**, L12 (2017), arXiv:1710.05833 [astro-ph.HE].
- [62] A. E. Romano and M. Sakellariadou, Mirage of Luminally Modified Gravitational-Wave Propagation, *Phys. Rev. Lett.* **130**, 231401 (2023), arXiv:2302.05413 [gr-qc].
- [63] A. Nishizawa, Generalized framework for testing gravity with gravitational-wave propagation. I. Formulation, *Phys. Rev. D* **97**, 104037 (2018), arXiv:1710.04825 [gr-qc].
- [64] S. Arai and A. Nishizawa, Generalized framework for testing gravity with gravitational-wave propagation. II. Constraints on Horndeski theory, *Phys. Rev. D* **97**, 104038 (2018), arXiv:1711.03776 [gr-qc].
- [65] L. Amendola, I. Sawicki, M. Kunz, and I. D. Saltas, Direct detection of gravitational waves can measure the time variation of the Planck mass, *JCAP* **08**, 030, arXiv:1712.08623 [astro-ph.CO].
- [66] T. Zhu, W. Zhao, J.-M. Yan, Y.-Z. Wang, C. Gong, and A. Wang, Constraints on parity and Lorentz violations in gravity from GWTC-3 through a parametrization of modified gravitational wave propagations, *Phys. Rev. D* **110**, 064044 (2024), arXiv:2304.09025 [gr-qc].
- [67] B.-Y. Zhang, T. Zhu, J.-F. Zhang, and X. Zhang, Forecasts for constraining Lorentz-violating damping of gravitational waves from compact binary inspirals, *Phys. Rev. D* **109**, 104022 (2024), arXiv:2402.08240 [gr-qc].
- [68] E. Belgacem, Y. Dirian, S. Foffa, and M. Maggiore, Non-local gravity. Conceptual aspects and cosmological predictions, *JCAP* **03**, 002, arXiv:1712.07066 [hep-th].
- [69] E. Belgacem, Y. Dirian, S. Foffa, and M. Maggiore, Gravitational-wave luminosity distance in modified gravity theories, *Phys. Rev. D* **97**, 104066 (2018), arXiv:1712.08108 [astro-ph.CO].
- [70] E. Bellini and I. Sawicki, Maximal freedom at minimum cost: linear large-scale structure in general modifications of gravity, *JCAP* **07**, 050, arXiv:1404.3713 [astro-ph.CO].
- [71] E. V. Linder, G. Sengör, and S. Watson, Is the Effective Field Theory of Dark Energy Effective?, *JCAP* **05**, 053, arXiv:1512.06180 [astro-ph.CO].
- [72] E. Bellini, A. J. Cuesta, R. Jimenez, and L. Verde, Constraints on deviations from  $\Lambda$ CDM within Horndeski gravity, *JCAP* **02**, 053, [Erratum: *JCAP* **06**, E01 (2016)], arXiv:1509.07816 [astro-ph.CO].
- [73] J. Noller and A. Nicola, Cosmological parameter constraints for Horndeski scalar-tensor gravity, *Phys. Rev. D* **99**, 103502 (2019), arXiv:1811.12928 [astro-ph.CO].
- [74] M. Ishak *et al.*, Modified gravity constraints from the full shape modeling of clustering measurements from DESI 2024, *JCAP* **09**, 053, arXiv:2411.12026 [astro-ph.CO].
- [75] J. M. Ezquiaga, Hearing gravity from the cosmos: GWTC-2 probes general relativity at cosmological scales, *Phys. Lett. B* **822**, 136665 (2021), arXiv:2104.05139 [astro-ph.CO].
- [76] A. Finke, S. Foffa, F. Iacovelli, M. Maggiore, and M. Mancarella, Probing modified gravitational wave propagation with strongly lensed coalescing binaries, *Phys. Rev. D* **104**, 084057 (2021).
- [77] H. Narola, J. Janquart, L. Haegel, K. Haris, O. A. Hannuksela, and C. Van Den Broeck, How well can modified gravitational wave propagation be constrained with strong lensing?, *Phys. Rev. D* **109**, 084064 (2024), arXiv:2308.01709 [gr-qc].
- [78] A. Garoffolo, G. Tasinato, C. Carbone, D. Bertacca, and S. Matarrese, Gravitational waves and geometrical optics in scalar-tensor theories, *JCAP* **11**, 040, arXiv:1912.08093 [gr-qc].
- [79] G. Tasinato, A. Garoffolo, D. Bertacca, and S. Matarrese, Gravitational-wave cosmological distances in scalar-tensor theories of gravity, *JCAP* **06**, 050, arXiv:2103.00155 [gr-qc].
- [80] E. Wempe, L. V. E. Koopmans, A. R. A. C. Wierda, O. A. Hannuksela, and C. van den Broeck, On the detection and precise localization of merging black holes events through strong gravitational lensing, *Mon. Not. Roy. Astron. Soc.* **530**, 3368 (2024), arXiv:2204.08732 [astro-ph.HE].
- [81] Y. Mellier *et al.* (Euclid), Euclid. I. Overview of the Euclid mission, *Astron. Astrophys.* **697**, A1 (2025), arXiv:2405.13491 [astro-ph.CO].
- [82] LSST Science Collaboration, P. A. Abell, *et al.*, LSST Science Book, Version 2.0, arXiv e-prints, arXiv:0912.0201 (2009), arXiv:0912.0201 [astro-ph.IM].
- [83] C. Karathanasis, B. Revenu, S. Mukherjee, and F. Stachurski, GWSim: Python package for creating mock GW samples for different astrophysical populations and cosmological models of binary black holes, *Astron. Astrophys.* **677**, A124 (2023), [Erratum: *Astron. Astrophys.* **682**, C1 (2024)], arXiv:2210.05724 [astro-ph.CO].
- [84] B. P. Abbott *et al.* (KAGRA, LIGO Scientific, Virgo), Prospects for observing and localizing gravitational-wave transients with Advanced LIGO, Advanced Virgo and KAGRA, *Living Rev. Rel.* **19**, 1 (2016), arXiv:1304.0670 [gr-qc].
- [85] Y.-Y. Choi, C. Park, and M. S. Vogeley, Internal and Collective Properties of Galaxies in the Sloan Digital Sky Survey, *Astrophys. J.* **658**, 884 (2007), arXiv:astro-ph/0611607.
- [86] S. Geng, S. Cao, Y. Liu, T. Liu, M. Biesiada, and Y. Lian, The velocity dispersion function of early-type galaxies and its redshift evolution: the newest results from lens redshift test, *Mon. Not. Roy. Astron. Soc.* **503**, 1319 (2021), arXiv:2102.12140 [astro-ph.GA].
- [87] G. Ferrami and J. S. B. Wyithe, Velocity dispersion function evolution from strong lensing statistics, *Mon. Not. Roy. Astron. Soc.* **537**, 779 (2025), arXiv:2410.20892 [astro-ph.GA].
- [88] A. K. Weigel, K. Schawinski, and C. Brudeker, Stellar mass functions: methods, systematics and results for the local Universe, *Mon. Not. Roy. Astron. Soc.* **459**, 2150 (2016), arXiv:1604.00008 [astro-ph.GA].
- [89] A. Abate *et al.* (LSST Dark Energy Science), Large Synoptic Survey Telescope: Dark Energy Science Collaboration 10.2172/1156445 (2012), arXiv:1211.0310 [astro-ph.CO].
- [90] K. Gilmore, S. Kahn, M. Nordby, D. Burke, P. O'Connor, J. Oliver, V. Radeka, T. Schalk, and R. Schindler, The lsst camera overview, (2006).

- [91] G. Pratten *et al.*, Computationally efficient models for the dominant and subdominant harmonic modes of precessing binary black holes, *Phys. Rev. D* **103**, 104056 (2021), arXiv:2004.06503 [gr-qc].
- [92] M. J. Williams, J. Veitch, and C. Messenger, Nested sampling with normalizing flows for gravitational-wave inference, *Phys. Rev. D* **103**, 103006 (2021), arXiv:2102.11056 [gr-qc].
- [93] M. J. Williams, J. Veitch, and C. Messenger, Importance nested sampling with normalising flows, *Mach. Learn. Sci. Tech.* **4**, 035011 (2023), arXiv:2302.08526 [astro-ph.IM].
- [94] G. Ashton *et al.*, BILBY: A user-friendly Bayesian inference library for gravitational-wave astronomy, *Astrophys. J. Suppl.* **241**, 27 (2019), arXiv:1811.02042 [astro-ph.IM].
- [95] D. Foreman-Mackey, D. W. Hogg, D. Lang, and J. Goodman, emcee: The MCMC Hammer, *Publ. Astron. Soc. Pac.* **125**, 306 (2013), arXiv:1202.3665 [astro-ph.IM].
- [96] S. Birrer, A. Amara, and A. Refregier, Gravitational Lens Modeling with Basis Sets, *Astrophys. J.* **813**, 102 (2015), arXiv:1504.07629 [astro-ph.CO].
- [97] M. Wright, J. Janquart, and M. Hendry, Determination of Lens Mass Density Profile from Strongly Lensed Gravitational-wave Signals, *Astrophys. J.* **959**, 70 (2023), arXiv:2307.07852 [astro-ph.HE].
- [98] S. Jana, S. J. Kapadia, T. Venumadhav, and P. Ajith, Cosmography Using Strongly Lensed Gravitational Waves from Binary Black Holes, *Phys. Rev. Lett.* **130**, 261401 (2023), arXiv:2211.12212 [astro-ph.CO].
- [99] S. Jana, S. J. Kapadia, T. Venumadhav, S. More, and P. Ajith, Strong-lensing cosmography using third-generation gravitational-wave detectors, *Class. Quant. Grav.* **41**, 245010 (2024), arXiv:2405.17805 [gr-qc].
- [100] K. N. Maity, S. Jana, T. Venumadhav, A. Barsode, and P. Ajith, Strong lensing cosmography using binary-black-hole mergers: Prospects for the near future, (2025), arXiv:2512.15168 [gr-qc].
- [101] X. Ying and T. Yang, Precision Joint Constraints on Cosmology and Gravity Using Strongly Lensed Gravitational Wave Populations, (2025), arXiv:2505.09507 [gr-qc].
- [102] S. Mukherjee, B. D. Wandelt, and J. Silk, Probing the theory of gravity with gravitational lensing of gravitational waves and galaxy surveys, *Mon. Not. Roy. Astron. Soc.* **494**, 1956 (2020), arXiv:1908.08951 [astro-ph.CO].
- [103] A. Balaudo, A. Garoffolo, M. Martinelli, S. Mukherjee, and A. Silvestri, Prospects of testing late-time cosmology with weak lensing of gravitational waves and galaxy surveys, *JCAP* **06**, 050, arXiv:2210.06398 [astro-ph.CO].
- [104] P. Madau and M. Dickinson, Cosmic Star Formation History, *Ann. Rev. Astron. Astrophys.* **52**, 415 (2014), arXiv:1403.0007 [astro-ph.CO].
- [105] R. K. Sheth *et al.* (SDSS), The Velocity Dispersion Function of Early-Type Galaxies, *Astrophys. J.* **594**, 225 (2003), arXiv:astro-ph/0303092.
- [106] M. Oguri, Y. Suto, and E. L. Turner, Gravitational lensing magnification and time delay statistics for distant supernovae, *Astrophys. J.* **583**, 584 (2003), arXiv:astro-ph/0210107.